Adsorption (2007) 13: 357–372
DOI 10.1007/s10450-007-9028-2

Multiphysics modeling of electric-swing adsorption system with in-vessel condensation

Menka Petkovska · Danijela Antov-Bozalo · Ana Markovic · Patrick Sullivan

Received: 30 April 2007 / Revised: 20 July 2007 / Accepted: 23 July 2007 / Published online: 22 September 2007

Abstract Mathematical modeling of an Electric-Swing Adsorption (ESA) system (adsorption cycle with electrothermal desorption step, performed by direct heating of the adsorbent particles by passing electric current through them), with annular, radial-flow, cartridge-type fixed-bed and in-vessel condensation, is performed by using Comsol Multiphysics™ software. Three multiphysics models are built, in order to describe three stages of a compete ESA cycle: adsorption, electrothermal desorption before the start of condensation and electrothermal desorption with in-vessel condensation. In order to describe the complete ESA cycle the models for the three stages are integrated, by using a combination of Comsol Multiphysics™ and Matlab™. The models were successfully used for simulation of separate stages of the process and of the complete ESA cycles, as well as for investigation of the influences of the main operational parameters on the process performance.

Keywords Multiphysics modeling · Electric-Swing Adsorption (ESA) · Electrothermal desorption · In-vessel condensation

The views and conclusions contained herein are those of the author and should not be interpreted as necessarily representing the official policies or endorsements, either expressed or implied, of the Air Force Office of Scientific Research or the U.S. Government.

M. Petkovska (✉) · D. Antov-Bozalo · A. Markovic
Department of Chemical Engineering, Faculty of Technology and Metallurgy, University of Belgrade, Belgrade, Serbia
e-mail: menka@tmf.bg.ac.yu

Present address:
A. Markovic
Max-Planck Institute for Dynamics of Complex Technical Systems, Sandtorstr. 1, 39106 Magdeburg, Germany

P. Sullivan
Air Force Research Laboratory, Tyndall AFB, FL, USA

Abbreviations

a (m^2/m^3)	Specific surface area
b (K^{-1})	Temperature coefficient of the bed electrical resistivity
C (mol/mol)	Adsorbate concentration in the gas phase
C^*(mol/mol)	Adsorbate concentration in the gas phase in equilibrium with the solid phase
C_{break} (mol/mol)	Breakthrough concentration
C_{sat} (mol/mol)	Saturation concentration
c_{pg} (J/mol/K)	Specific heat capacity of the inert gas
c_{pl} (J/mol/K)	Specific heat capacity of liquid adsorbate
c_{ps} (J/g/K)	Heat capacity of the solid phase
c_{pv} (J/mol/K)	Specific heat capacity of gaseous adsorbate
D_m (mol/cm/s)	Mass transfer dispersion coefficient
D_t^{hg} (W/K/cm)	Heat diffusivity of the gas phase
D_t^{hs} (W/K/cm)	Heat diffusivity of the solid phase
E (J/mol)	Adsorption energy of the adsorbate (D-R equation)
g (cm/s^2)	Gravitation constant
G (mol/s)	Flow rate of the inert gas
H (cm)	Bed axial dimension (Fig. 2)
h_1 (cm)	Adsorber dimension (Fig. 2)
h_b ($J/cm^2/K$)	Solid to gas heat transfer coefficient within the bed

h_{s1} (J/cm^2/K)	Heat transfer coefficient from the solid phase to the gas phase in the central tube(s)
h_{s2} (J/cm^2/K)	Heat transfer coefficient from the solid phase to the gas phase in the annular tube
h_{wg} (J/cm^2/K)	Gas to ambient heat transfer coefficient (heat losses)
J (A/cm^2)	Current density
J_{cond} (mol/cm^2/s)	Condensation flux
k (cm^2)	Asorbent bed permeability
k_m (mol/cm^2/s)	Mass transfer coefficient in the adsorbent bed
k_{m1} (mol/cm^2/s)	Mass transfer coefficient between the adsorbent bed and the gas in the central tube
k_{m2} (mol/cm^2/s)	Mass transfer coefficient between the adsorbent bed and the gas in the annular tube
$\dot{L}_{cond}$ (mol/s)	Flow-rate of the condensed liquid
L_{cond} (mol)	Total amount of the condensed liquid
p (Pa)	Gas pressure
p_a (Pa)	Ambient pressure
p_c (Pa)	Critical pressure
p^0 (Pa)	Adsorbate saturation pressure
$\dot{Q}_{el}$ (W)	Rate of heat generation (equal to electric power)
Q_{el} (J)	Heat generation (equal to electric energy)
q (mol/g)	Adsorbate concentration in the solid phase
R_g (J/mol/K)	Gas constant
r (cm)	Radial coordinate
r_1 (cm)	Adsorber dimension—radius of the central tube (Fig. 2)
r_2 (cm)	Adsorber dimension (Fig. 2)
r_3 (cm)	Adsorber dimension (Fig. 2)
r_4 (cm)	Adsorber dimension—radius of the adsorber vessel (Fig. 2)
S_w (cm^2)	Surface are of the outer wall of the adsorber vessel
T_a (K)	Ambient temperature
T_g (K)	Gas phase temperature
T_c (K)	Critical temperature
T_R (K)	Referent temperature
T_s (K)	Solid phase temperature
T_{sw} (K)	Switch temperature (from desorption to adsorption)
T_w (K)	Wall temperature
t (s)	Time
U (V)	Electric potential
U_0 (V)	Supply voltage
u (cm/s)	Radial superficial gas velocity
VP_A, VP_B, VP_C, VP_D	Wagner constants (Wagner equation)
v (cm/s)	Axial superficial gas velocity
W_0 (cm^3/g)	Total volume of micropores (D-R equation)
z (cm)	Axial coordinate

Greek letters:

α_p	Purification factor
α_s	Separation factor
ΔH_{ads} (J/mol)	Heat of adsorption
ΔH_{cond} (J/mol)	Heat of condensation
ε_b	Bed porosity
μ (Pa/s)	Dynamic viscosity
ρ (Ωcm)	Electric resistivity
ρ_0 (Ωcm)	Electric resistivity at referent temperature T_R
ρ_g (mol/cm^3)	Gas phase density
ρ_b (g/cm^3)	Adsorbent bed density
ρ_A (g/cm^3)	Adsorbate density
τ (s)	Time period

Subscripts:

A	Adsorption
b	Bed
D	Desorption
g	Gas
in	Inlet
out	Outlet
p	Previous (initial)
r	In the radial (r) direction
s	Solid phase
ct	Central tube
as	Annular space
z	In the axial (z) direction

Special characters:

$\langle\ \rangle$	Time average value

1 Introduction

Electric (or electrothermal) swing adsorption (ESA) is a relatively new name (Yu et al. 2007; Sullivan et al. 2004a) for an essentially temperature-swing adsorption (TSA) cycle in which the adsorbent material is heated by passing electric current through it (owing to Joule effect).

The idea about regeneration of used adsorbent beds by direct heating by electric current was first published in the 1970s (Fabuss and Dubois 1970). The desorption process based on this principle was later named electrothermal desorption (Petkovska et al. 1991) and it was recognized as a

prospective way to perform desorption steps of TSA cycles (Petkovska et al. 1991).

The main differences between electrothermal desorption and classical techniques of thermal regeneration of used adsorbents (e.g. heating by hot gas or steam) are (Sullivan 2003; Petkovska and Mitrović 1994a, 1994b):

- Energy efficiency is higher than when heating by steam or inert gas, because the energy is delivered directly to the adsorbent, thus minimizing the energy expended for heating of the vessel and ancillary equipment.
- Heating rate of the adsorbent is not limited by heat/mass transfer rates between the carrier gas and the adsorbent, because the energy is directly applied to the adsorbent rather than being delivered by the carrier gas stream.
- Effluent concentration of adsorbate can be maximized, because the purge gas flow rate is controlled independently from the power applied to the adsorbent.
- Unlike steam regeneration, no water is introduced into the system, which is difficult and costly to separate from water-miscible adsorbates, and which can cause corrosion.
- The directions of heat and mass transfer are identical in the case of electrothermal desorption, and opposite in the case of conventional thermal desorption by hot gas or steam. This can influence the process kinetics and dynamics.

It was shown that electrothermal desorption has some advantages over conventional methods, regarding adsorption kinetics and dynamics (Petkovska and Mitrović 1994a, 1994b) and energy efficiency (Petkovska et al. 1991; Sullivan 2003).

Most applications of electrothermal desorption have been based on fibrous activated carbon materials (Petkovska et al. 1991; Rood et al. 2002; Sullivan et al. 2001, 2004a, 2004b; Subrenat and Le Cloirec 2004, 2006; Moon and Shim 2006; Luo et al. 2006), although granular activated carbons (Snyder and Leesch 2001; Sushchev et al. 2002; Luo et al. 2006) and, recently, carbon monoliths (Luo et al. 2006; Yu et al. 2002, 2007), have also been used.

Up to now, different applications (mostly on laboratory scale) of regeneration of used adsorbents by electrothermal desorption have been reported: air purification, with emphases on removal of hazardous volatile organic compounds (Baudu et al. 1992; Azou et al. 1993; Sullivan et al. 2001, 2003; Subrenat and Le Cloirec 2006), gas separation (Moon and Shim 2006) and solvent recovery (Bathen et al. 1997; Lordgooei et al. 1996; Snyder and Leesch 2001; Sullivan 2003). In the last couple of years, some applications of electrothermal desorption on industrial scale have also been reported (Bathen 2002; Subrenat and Le Cloirec 2004, 2006).

The subject of this investigation is mathematical modeling of an ESA system based on assembly of annular, radial-flow, cartridge-type fixed-beds, with in-vessel condensation (Rood et al. 2002; Sullivan 2003; Sullivan et al. 2004a), which has been developed for removal and recovery of hazardous volatile organic compounds. This system involves a large number of coupled processes and phenomena: fluid flows through tubes and porous beds, adsorption, mass transfer, heat transfer, heat generation associated with electric current flow, and condensation, all in a rather complex geometry. Such a system is very demanding from the modeling point of view and represents a good candidate for multiphysic modeling. This manuscript presents the procedure and results of mathematical modeling of this system by using Comsol Multiphysics™, a software tool specialized for multiphysics modeling.

2 Description of the modeled system

The adsorber of the ESA system treated in this work contains one cartridge-type adsorption bed. It is schematically shown in Fig. 1a. The cartridge, which is schematically shown in Fig. 1b, is formed as a cylindrical roll of activated carbon fiber cloth, spirally coiled around a porous central pipe used for introducing the gas stream (the stream that has to be purified, during adsorption, or an inert gas stream, during desorption). The gas flow through the adsorption bed is in the radial direction.

During the desorption step, a low flow-rate stream of pure inert is introduced into the adsorber and, at the same time, electric current is passed through the adsorbent bed in the axial direction, causing heat generation, heating of the bed and desorption. The desorbed vapor is carried by the radially flowing gas stream towards the adsorber wall. When the vapor concentration near the wall becomes equal to the saturation concentration corresponding to the wall temperature, the vapor is condensed and drained out of the system through the funnel shaped bottom outlet (see Fig. 1a).

The switching between adsorption and desorption is performed when the outlet concentration reaches some predefined breakthrough value. In order to avoid thermal degradation of the adsorbate, the desorption step is ended by turning the electric heating off when the temperature in the adsorbent bed reaches some predefined maximal temperature.

The following assumptions were used in setting up the models:

- The adsorbent bed is treated as homogeneous, with uniform adsorbent porosity and density.
- The mass and heat transfer resistances on the particle scale are neglected.
- The fluid phase is treated as an ideal gas mixture of an inert and a single adsorbate.

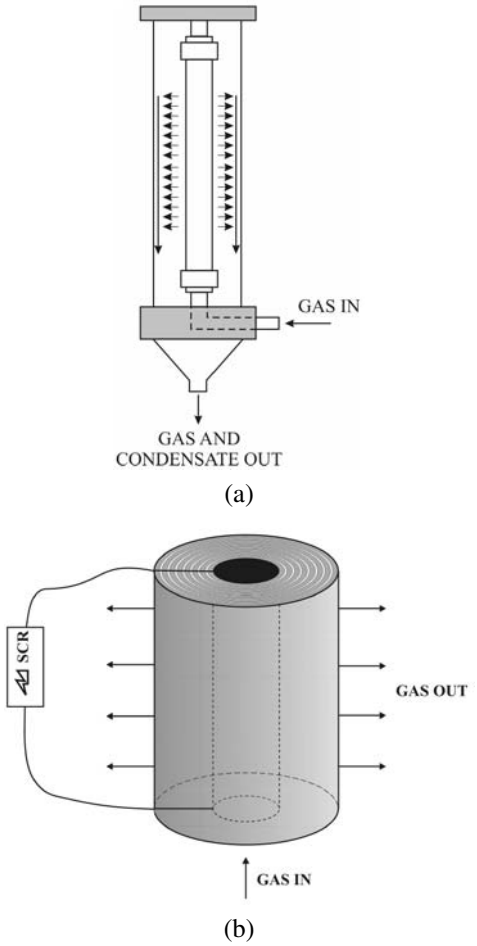

Fig. 1 Schematic representation of: (**a**) the adsorber with cartridge-type adsorbent bed and in-vessel condensation; and (**b**) the annular, radial-flow cartridge

- The electric resistivity of the adsorbent is temperature dependent. Linear temperature dependence is assumed, based on experimental results reported in (Sullivan 2003).
- All other physical parameters and coefficients are considered as constants.
- The condensation at the adsorber wall is dropwise. This assumption is based on experimental observations reported in Sullivan (2003).
- The volume of the condensed liquid is neglected, i.e., it is assumed that the liquid drops don't influence the gas flow.
- The heat resistance and heat capacity of the adsorber wall are neglected, so the wall temperature is regarded as equal to the temperature of the environment.
- Heat transfer by radiation is neglected.
- The electric power during electrothermal desorption is supplied under constant voltage conditions.

3 Multiphysics models for separate steps of the ESA cycle

Analysis of the adsorber defined in the previous section shows that it consists of three parts: the central tube used for introducing the gas, the adsorbent bed and the annular space between the adsorbent bed and the outer adsorber wall. Also, three consecutive steps of the complete ESA cycle with in-vessel condensation can be defined:

- Adsorption;
- Desorption without condensation;
- Desorption accompanied with condensation.

The last two steps are parts of the desorption half-cycle.

The mathematical model of the system consists of the momentum, mass and heat balances for different parts of the system (the central tube of the cartridge, the adsorbent bed and the annular space around the cartridge) and for the gas and solid phases, as well as the balance equation defining electric current flow and heat generation owing to Joule's effect.

In addition, the Dubinin–Radushkevich (D-R) equation (Dubinin 1989) is used to calculate the adsorption equilibrium in this system.

In principle all three steps of the ESA cycle can be described by the same set of model equations. Nevertheless, the heat balance for the solid phase and the boundary conditions corresponding to different steps can be different, so it was necessary to build three different models. Let us name the models for adsorption, desorption and desorption with condensation: Model_A, Model_D and Model_DC, respectively.

In order to reduce the model complexity, and using the fact that the adsorber is practically axially symmetrical, the Comsol Multiphysics models were built in the *axially symmetrical 2D space*. The model geometry, which is identical for all three models, is shown in Fig. 2. As can be seen from this figure, the model is defined for only one half of the adsorber, and the other half is axially symmetrical. In that way, the number of the needed mesh elements is reduced to half, which dramatically reduces the computational time. In Fig. 2, we also define the main adsorber dimensions and the sub-domains. Based on the structure of the adsorber, three sub-domains are defined (Fig. 2):

- S1—the central tube;
- S2—the adsorbent bed;
- S3—the annular space between the cartridge and the outer adsorber wall.

In the Comsol Multiphysics working environment, the model equations can be defined by choosing the appropriate application modes from a menu. The following application modes were used in our models:

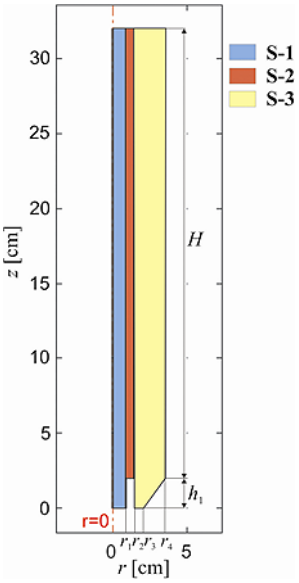

Fig. 2 Definition of the model geometry and sub-domains

1. *Non-isothermal flow*—for defining momentum balances and fluid flows in tubes (in our models defined in sub-domains S1 and S3);
2. *Brinkman Equations*—for defining momentum balances and fluid flows in packed beds (in sub-domain S2);
3. *Convection and Diffusion*—for defining mass transfer in flowing fluids (in all three sub-domains);
4. *Diffusion*—for defining mass transfer in stagnant phases (in sub-domain S2);
5. *Convection and Conduction*—for defining heat transfer in flowing fluids (in all three sub-domains);
6. *Heat transfer by Conduction*—for defining heat transfer in stagnant phases (in sub-domain S2);
7. *Conductive Media DC*—for defining electric current flow and heat generation by Joule's effect (in sub-domain S2).

In principle, the Conductive Media DC application mode needs to be defined only in Model_D and Model_DC, corresponding to the parts of the ESA cycle when the electricity is on. Nevertheless, in order to integrate the three models into a model of the complete ESA cycle, this application mode was used in all three models.

The complete mathematical model of our system is too cumbersome for presenting it here. The model equations are listed in Appendix 1. Here we only point out the main differences between the three models:

1. The energy balance for the solid phase ((20) from Appendix 1) contains a term defining the Joule heat generation ($\delta \dot{Q}_{el}/dV$). For Model_A this term is equal to zero.
2. The boundary conditions for the mass and heat balances corresponding to the adsorber wall are different in Model_A and Model_D on one hand (the parts of the process without condensation) and Model_DC, on the other hand (the part of the process with condensation). If no condensation at the adsorber wall is present, zero mass flux at the wall is assumed, while the heat flux is defined by heat losses (35). On the other hand, in the case of condensation, the boundary condition for the mass balance is defined by constant concentration (equal to the saturation concentration corresponding to the wall temperature), while an additional term defining the heat of condensation is added to the equation defining the boundary condition for the heat balance (36).

The seven application modes listed here define the velocities, concentrations and temperatures in all three sub-domains and both phases, as well as the electric potential and resistance of the adsorbent bed, as functions of time and space coordinates. Nevertheless, it is recommendable to define and calculate two additional parameters which characterize the ESA process: the mass of the condensed liquid per cycle and the used electric energy per cycle.

3.1 Calculation of the mass of the condensed liquid

The flux of the condensed liquid is calculated from the gas concentration gradient at the adsorber wall:

$$J_{cond}(z,t) = -D_{m,r}\frac{\partial C}{\partial r}\bigg|_{r=r_4}. \tag{1}$$

This flux is a function of the axial position z and time t (r is the radial coordinate, r_4 the radius of the adsorber vessel (see Fig. 2), C the gas concentration, and $D_{m,r}$ the radial diffusion coefficient of the gas phase). The condensation rate is calculated by integration of this flux over the whole surface of the adsorber wall, and is a function of time only:

$$\dot{L}_{cond}(t) = \int_0^{S_w} J_{cond}(z,t)dS. \tag{2}$$

The total amount of the condensed liquid is obtained by integrating the condensation rate over time:

$$L_{cond} = \int_0^{\tau_{cond}} \dot{L}_{cond}(t)dt. \tag{3}$$

S_w is the total surface area of the outer adsorber wall and τ_{cond} the total time of condensation.

3.2 Calculation of the used electric energy

The used electric energy is equal to the Joule heat produced in the adsorbent material. This energy per unit volume and unit time is:

$$\frac{\delta \dot{Q}_{el}}{dV} = \frac{1}{\rho}\left(\left(\frac{\partial U}{\partial r}\right)^2 + \left(\frac{\partial U}{\partial z}\right)^2\right) \tag{4}$$

where ρ is the electric resistivity, which is temperature dependent, and U the electric potential.

The used electric power is obtained by integration over the adsorbent bed volume:

$$\dot{Q}_{el}(t) = \int_{z=0}^{z=H} \int_{r=r_2}^{r=r_3} r \frac{1}{\rho} \left(\left(\frac{\partial U}{\partial r} \right)^2 + \left(\frac{\partial U}{\partial z} \right)^2 \right) 2\pi \, dr \, dz \tag{5}$$

and the total used energy during desorption, by integration over time:

$$Q_{el} = \int_0^{\tau_{des}} \dot{Q}_{el}(t) dt. \tag{6}$$

τ_{des} is the total desorption time and H, r_2 and r_3 the adsorber dimensions defined in Fig. 2.

4 Model of the complete ESA cycle

In order to simulate the complete ESA cycle, the three Comsol Multiphysics models defined in the previous section have to be run in a sequence, with automatic switching from one model to the next one when certain predefined conditions are met. The following switches need to be performed:

- *Switching from Model_A to Model_D.* This switch corresponds to the end of adsorption and start of a new desorption step. It is performed automatically when the outlet concentration reaches a certain predefined breakthrough value C_{break}. The outlet concentration is obtained as the average value across the outlet, although the simulation results showed that the gas concentration across the outlet is nearly uniform.
- *Switching from Model_D to Model_DC.* This switch is performed at the moment when the gas concentration at the adsorber wall becomes equal to the saturation concentration corresponding to the wall temperature C_{sat}, resulting with the start of condensation. The saturation concentration is calculated using the Wagner equation (Reid et al. 1987). The simulations show that condensation practically starts at the same time at the whole surface of the outer wall of the adsorber.
- *Switching from Model_DC to Model_A.* This switch defines the end of desorption and start of a new adsorption part of the cycle. It is performed when the maximal temperature in the adsorbent bed reaches certain predefined value T_{sw}, which should not be exceeded, and the electricity is switched off. The modeled ESA cycle does not assume a cooling step between the end of heating and start of the new adsorption step (Sullivan 2003).

Although in principle different Comsol Multiphysics models can be run consecutively, automatic switching from one model to another, by checking whether certain conditions are met, is not possible in Comsol Multiphysics. The problem was solved by using the coherence of Comsol Multiphysics and Matlab. All three Comsol Multiphysics models were saved as Matlab m-files and then integrated into one Matlab model, defining the complete cycle. The structure of this integral model is shown in Fig. 3.

In this figure, as well as in our program, the cycle is started with the desorption step, with an equilibrium initial state in which the temperatures of both phases are equal (and equal to the temperature of the environment) and the adsorbent bed is assumed to be saturated, in equilibrium with the inlet gas concentration during the adsorption step. This sequence was chosen because it results with much faster establishing of the cyclic steady-state (in only 2–3 cycles), compared to the case when the process is started with the adsorption step, from an initially clean adsorbent bed.

In order to enable integration of the models, the same application modes have to be defined in all three Comsol Multiphysics models, in exactly the same sequence. Also, the model geometry and the mesh have to be identical in all three models. Actually, in our integral model the model segments corresponding to geometry definition and mesh initialization are defined only once (Fig. 3).

5 Solution of the models and some simulation results

5.1 Used mesh, solvers and parameters

Comsol Multiphysics software is based on the finite element method for solving systems of coupled partial differential equations (PDEs) (Comsol AB 2005). The first step in the solution procedure is generation of the mesh for the finite element method. In our simulations we used a normal density mesh, with 568 mesh elements, which ensured a good compromise between high accuracy of the solution, without serious convergence problems on one, and moderate computational times, on the other hand.

The finite element method is actually a method of discretization which approximates the PDEs by large sets of ordinary differential equations (ODEs). The software offers a choice of different solvers for solving the resulting sets of ODEs. In our simulations we used the direct UMFPACK solver (Comsol AB 2005), which showed good results.

The models of the presented system were solved and used for simulation of separate stages and of the complete ESA cycles, for the following adsorber dimensions:

- Length of the cartridge: 30 cm
- Radius of the central tube of the cartridge: 0.95 cm
- Thickness of the adsorbent bed: 0.55 cm
- Radius of the adsorber vessel: 3.5 cm.

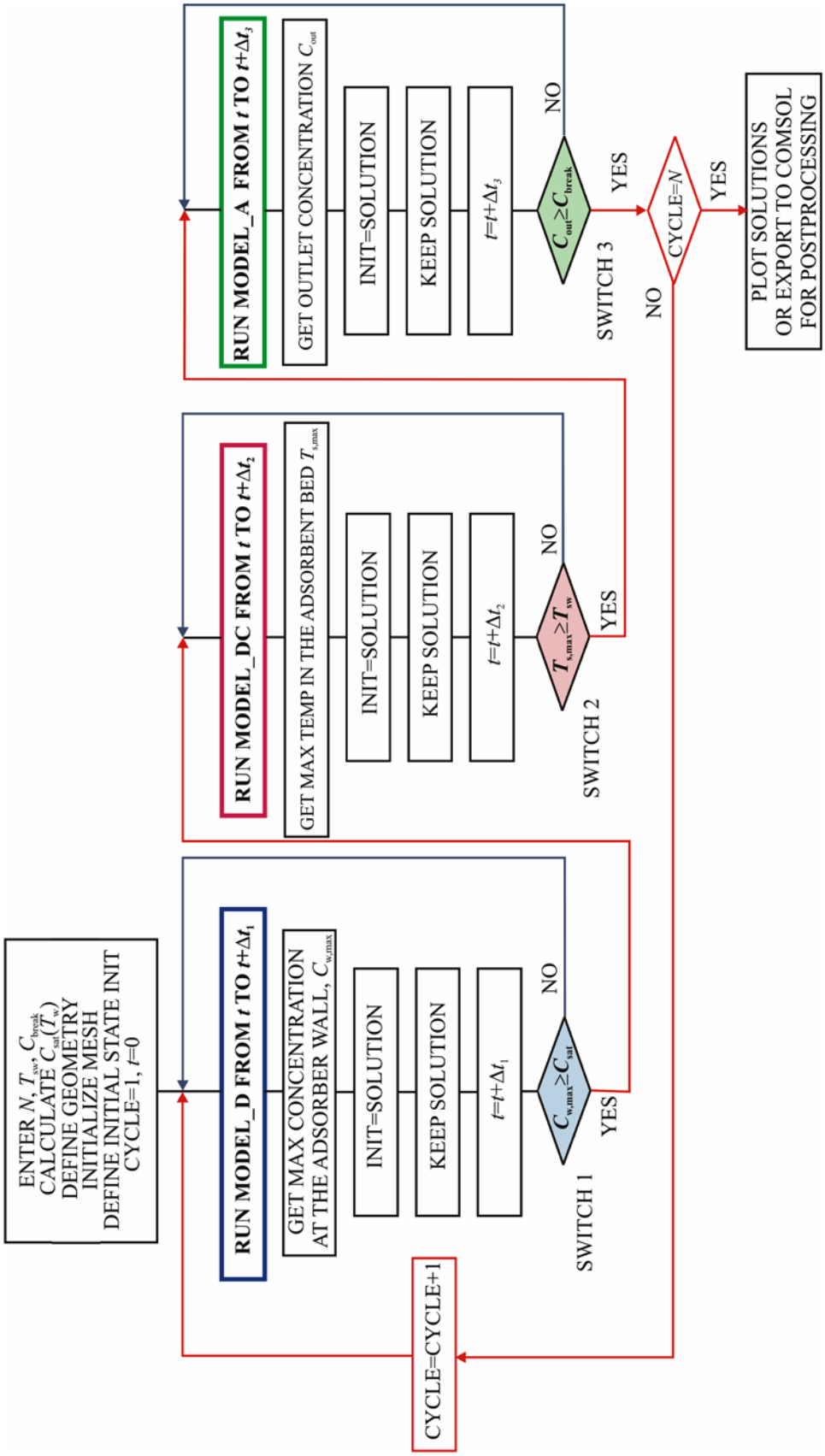

Fig. 3 A block scheme of the model of the complete ESA cycle and the corresponding Matlab program

The physical parameters in our models correspond to the following adsorption system (Sullivan 2003):

- Adsorbent: American Kynol ACC-5092-20 (activated carbon fiber cloth material)
- Adsorbate: methyl ethyl ketone (MEK)
- Carrier gas: nitrogen.

The simulations were performed for different switch temperatures, breakthrough concentrations, supply voltages and gas flow-rates during the adsorption and desorption half-cycles. The inlet concentration during adsorption was equal to the initial gas concentration (in all simulations 0.001 mol/mol). The initial, inlet gas and ambient temperatures were all equal (293.15 K).

The complete list of the model parameters, with their definitions and the numerical values used in the simulations is given in Appendix 2.

The software offers a variety of graphical representation of the data. We will give a small portion of the simulation results, as illustration.

5.2 Simulation results for separate stages

The developed Comsol Multiphysics models were first used for simulation of adsorption on a previously clean adsorbent and desorption from a previously saturated adsorbent bed. As a result, the gas velocities, pressures, concentrations and temperatures in all parts of the adsorber are simulated. Here are some of these results.

In Fig. 4, the gas velocities in all three subdomains are presented in vector form. The velocity profiles in the system are established very fast (during the first 2–3 seconds). After that, the velocities change somewhat, owing to the change of the gas temperature and concentration, but the changes of the velocity profiles are not significant. The results shown in Fig. 4 correspond to adsorption and $t = 7000$ s when the adsorption is complete. Very similar picture of the velocity profiles is obtained for desorption. Figure 4 shows that in the central tube and in the annular space the gas flows mainly in the axial direction, and through the adsorbent bed in the radial direction.

In Figs. 5 and 6, two samples of the simulation results, representing the gas and solid concentrations and temperatures, in the form of surface-plots, are given. The results presented in Fig. 5 correspond to adsorption, 200 s after the start of adsorption on a previously clean adsorbent, while the results in Fig. 6 correspond to desorption, 80 s

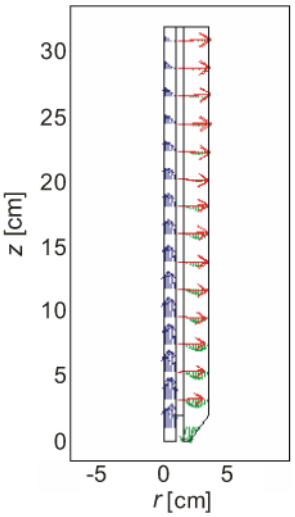

Fig. 4 The velocity profiles in all 3 sub-domains, in vector form

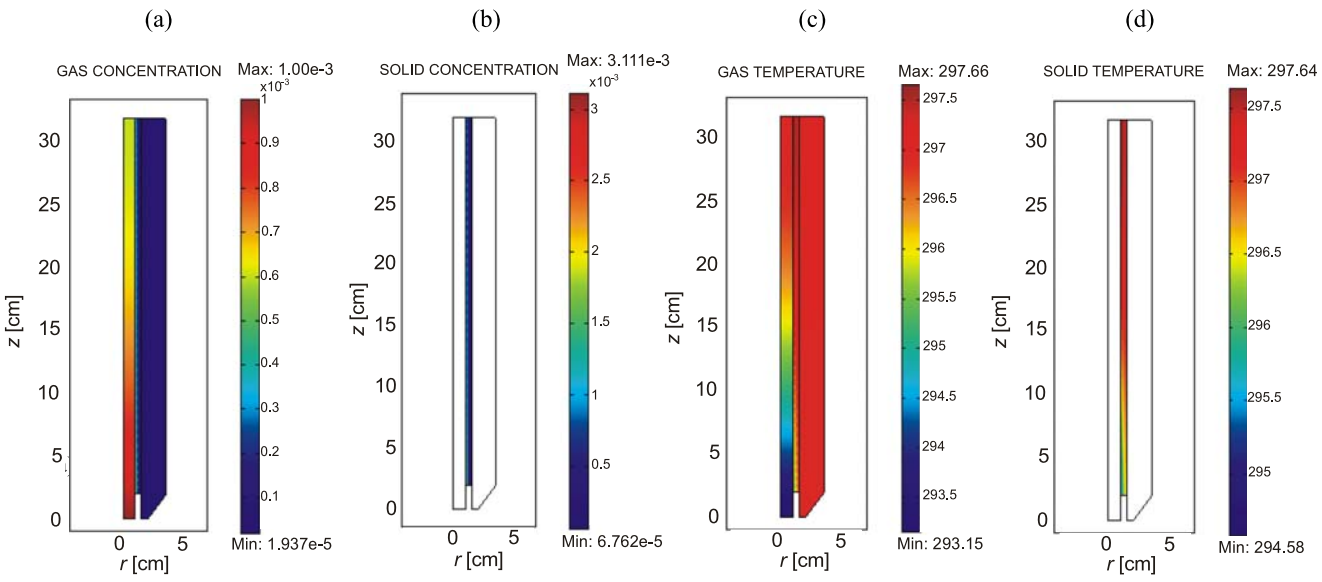

Fig. 5 Simulation of adsorption: (**a**) concentration of the gas phase; (**b**) concentration of the solid phase; (**c**) gas temperature; (**d**) solid temperature ($C_{in} = 0.001$ mol/mol, $G_A = 0.1$ mol/s, $t = 200$ s)

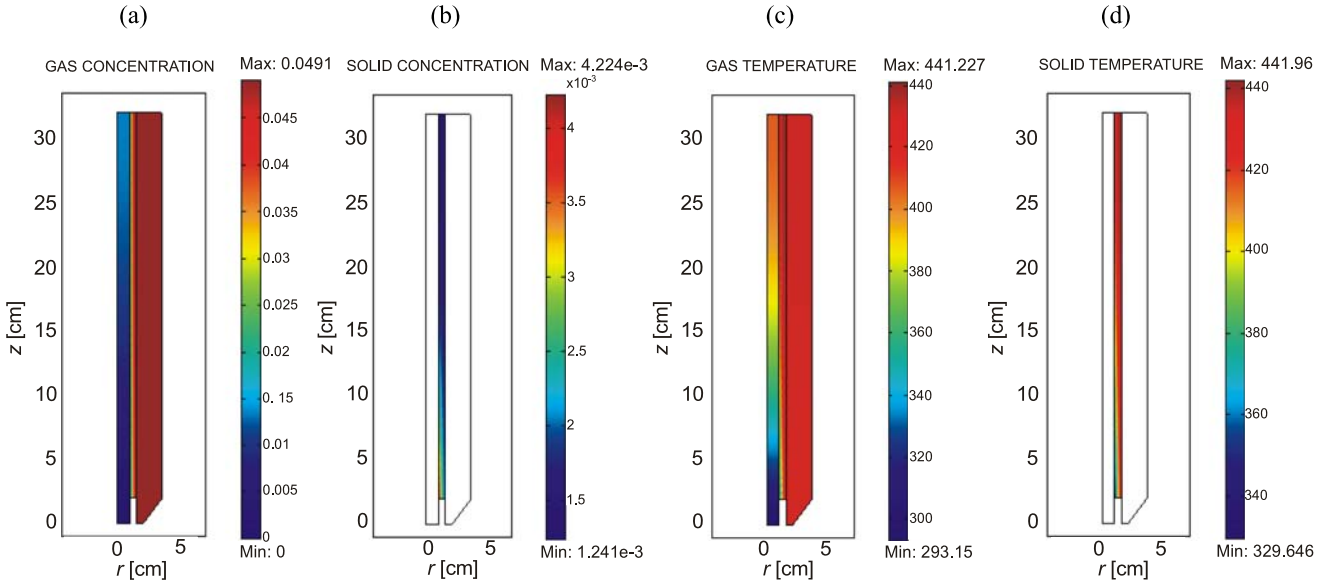

Fig. 6 Simulation of desorption: (**a**) concentration of the gas phase; (**b**) concentration of the solid phase; (**c**) gas temperature; (**d**) solid temperature ($C_p = 0.001$ mol/mol, $q_p = 0.00465$ mol/g, $U_0 = 11$ V, $G_D = 0.01$ mol/s, $t = 80$ s)

after the start of desorption from a previously saturated column.

By inspection of Figs. 5 and 6 it can be observed that the concentrations and temperatures change both in the axial and in the radial direction of the adsorber, both in the adsorbent bed and in the tubes. Accordingly, using simpler, one-dimensional model, which would neglect the changes in the axial direction and assuming perfect mixing of the gas in the tubes (Petkovska et al. 2005) would not be justified.

5.3 Simulation results of the ESA cycles

Simulation of the complete ESA process was performed by running the integral Matlab programme, obtained by integration the models of the three separate steps, as explained in Sect. 4. A sample of the simulation results of the first three ESA cycles, corresponding to switch temperature 463.15 K, breakthrough concentration 0.0005 mol/mol (50% of the feed concentration during adsorption), supply voltage 11 V and inert gas flow-rates during adsorption and desorption 0.1 mol/s and 0.01 mol/s, respectively, is presented in Figs. 7 (the outlet concentration), 8 (the maximal adsorbent temperature) and 9 (the condensation rate). All other parameters were the same as in the simulations of the separate adsorption and desorption steps.

It can be observed that after the second cycle a quasi-steady state is practically achieved. Also, very long adsorption and short desorption times are observed.

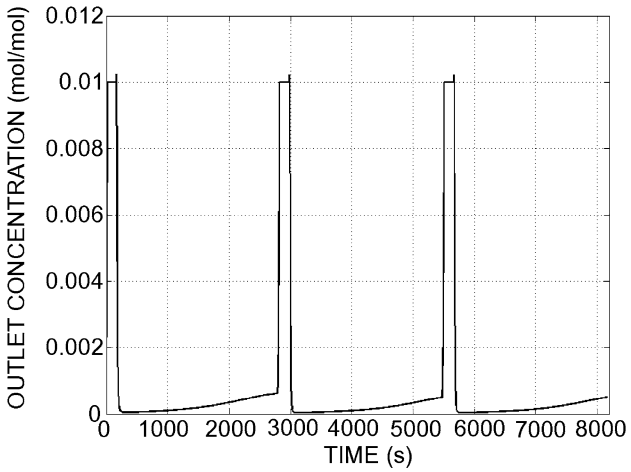

Fig. 7 The outlet concentration during ESA ($C_{in} = 0.001$ mol/mol, $U_0 = 11$ V, $G_A = 0.1$ mol/s, $G_D = 0.01$ mol/s, $T_{sw} = 463.15$ K and $C_{break} = 0.5C_{in}$)

6 Analysis of the influence of the process parameters as a basis for optimization of the ESA process

In order to analyze the performance of the ESA system, some performance criteria were first defined, as measures of the process quality:

- Adsorption time, τ_A
- Desorption time, τ_D
- Average outlet concentration during adsorption, $\langle C_{out} \rangle_A$
- Average outlet concentration during desorption, $\langle C_{out} \rangle_D$
- Separation factor—defined as the ratio of the average outlet concentrations during adsorption and desorption, α_s

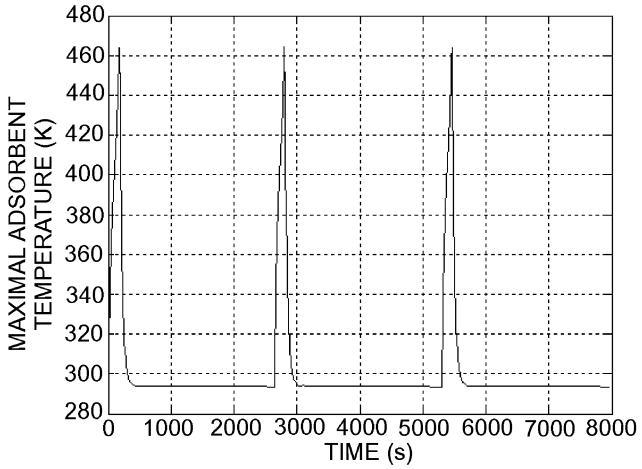

Fig. 8 The maximal adsorbent temperature during ESA ($C_{in} = 0.001$ mol/mol, $U_0 = 11$ V, $F_A = 0.1$ mol/s, $F_D = 0.01$ mol/s, $T_{sw} = 463.15$ K and $C_{break} = 0.5C_{in}$)

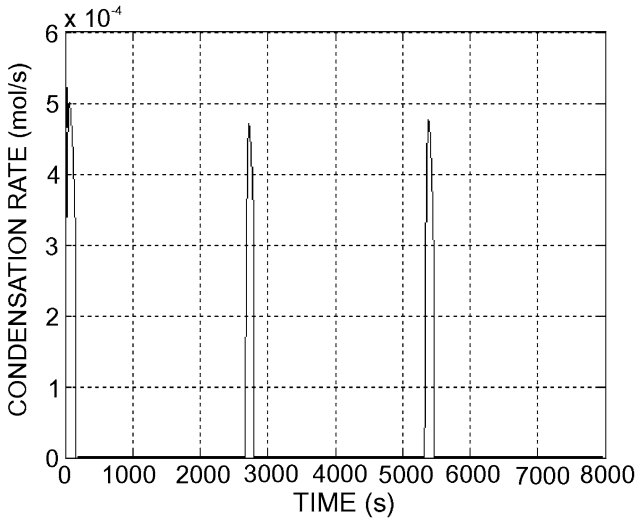

Fig. 9 The condensation rate during ESA ($C_{in} = 0.001$ mol/mol, $U_0 = 11$ V, $F_A = 0.1$ mol/s, $F_D = 0.01$ mol/s, $T_{sw} = 463.15$ K and $C_{break} = 0.5C_{in}$)

- Purification factor—defined as the ratio of the outlet and inlet concentrations during adsorption, α_p
- The total amount of condensed liquid per cycle, L_{cond}
- Total recovery, defined as the ratio of the total amount of condensed liquid and the amount of adsorbate entering the system during one cycle, $L_{cond}/(C_{in}\tau_A G_A)$
- Used electric energy per cycle, Q_{el}
- Used energy per mol of condensate, Q_{el}/L_{cond}.

The influence of the following operational parameters was analyzed:

- The switch temperature T_{sw};
- The breakthrough concentration C_{break};
- The electrical voltage during desorption U_0.

The results are shown in tabular form. The influence of the switch temperature on the defined performance criteria is shown in Table 1, the influence of the breakthrough concentration in Table 2 and the influence of the supply voltage in Table 3. All other parameters were identical to those used in Figs. 7–9.

The results given in these tables show clear influence of the chosen operational parameters on the performance of the ESA system. E.g., it could be concluded that the increase of the switch temperature is favorable from the point of view of separation and purification of the feed stream, as well as regeneration of the adsorbed vapor, but unfavorable from the point of view of energy consumption. On the other hand, the increase of the breakthrough concentration is unfavorable from the point of view of separation and purification of the feed stream, but favorable when regeneration of the adsorbed vapor and energy consumption are of main interest. The increase of the supply voltage results with higher energy efficiency (lower energy consumption per mole of condensate).

The total vapor recovery is ∼20% in almost all cases. It increases with the increase of the switch temperature, decrease of the breakthrough concentration and with the increase of the supply voltage. This value is somewhat underestimated, as our model assumes that condensation takes place only during the desorption half-cycle. Nevertheless, the simulations showed that the condensation process was not finished at the end of the desorption half-cycle, i.e., when the electricity was turned off. Consequently, condensation is expected to continue in the beginning of the adsorption-half cycle, until the gas concentration at the adsorber wall falls below its saturation value. In order to take this into account, another Comsol Multiphysics model would need to be incorporated, in which the heat generation term ($\delta \dot{Q}_{el}/dV$) in (20) is zero and the boundary conditions at the adsorber wall correspond to condensation (36).

7 Conclusions

In this paper we have shown that Comsol Multiphysics™, in combination with Matlab™, can be used for modeling and simulation of a complex adsorption cycle. Both the geometry and the phenomena involved in the modeled ESA process are very complex (3 sub-domains and 7 application modes). For the chosen mesh, the models were used without serious convergence problems, and with acceptable computing times. The integrated model of the complete ESA cycle was successfully used for simulation and investigation of the main operational parameters on the quality of the ESA process.

The current model was simplified in several ways. First, most physical and transport parameters were considered as

Table 1 Analysis of the influence of the switch temperature T_{sw}

Criterium	Switch temperature T_{sw} [K]		
	433.15	463.15	493.15
$\langle C_{out}\rangle_D$ [mol/mol]	0.00853	0.00879	0.00895
$\langle C_{out}\rangle_A$ [mol/mol]	2.65×10^{-4}	2.00×10^{-4}	1.84×10^{-4}
$\alpha_s = \langle C_{out}\rangle_D / \langle C_{out}\rangle_A$	32.189	43.950	48.641
$\alpha_p = \langle C_{out}\rangle_A / C_{in,A}$	0.265	0.200	0.184
L_{cond} [mol]	0.0400	0.0499	0.0557
$L_{cond}/(C_{in}\tau_A G_A)$ [%]	16.90	20.45	21.42
Q_{el} [KJ]	13.363	16.735	19.593
Q_{el}/L_{cond} [KJ/mol]	334.07	335.37	351.76
τ_D [s]	130	158	180
τ_A [s]	2370	2440	2600

Table 2 Analysis of the influence of the breakthrough concentration C_{break}

Criterium	Breakthrough concentration C_{break} [mol/mol]		
	2.5×10^{-4} (25% C_{in})	3.5×10^{-4} (35% C_{in})	5.0×10^{-4} (50% C_{in})
$\langle C_{out}\rangle_D$ [mol/mol]	0.00835	0.00854	0.00879
$\langle C_{out}\rangle_A$ [mol/mol]	1.28×10^{-4}	1.58×10^{-4}	2.00×10^{-4}
$\alpha_s = \langle C_{out}\rangle_D / \langle C_{out}\rangle_A$	65.234	54.051	43.950
$\alpha_p = \langle C_{out}\rangle_A / C_{in,A}$	0.128	0.158	0.200
L_{cond} [mol]	0.0397	0.0437	0.0499
$L_{cond}/(C_{in}\tau_A G_A)$ [%]	22.06	21.69	20.45
Q_{el} [KJ]	15.268	15.717	16.735
Q_{el}/L_{cond} [KJ/mol]	384.58	359.66	335.37
τ_D [s]	143	148	158
τ_A [s]	1800	2050	2440

Table 3 Analysis of the influence of the voltage used for desorption, U_0

Criterium	Supply voltage U_0 [V]		
	10	11	12
$\langle C_{out}\rangle_D$ [mol/mol]	0.00895	0.00879	0.00869
$\langle C_{out}\rangle_A$ [mol/mol]	1.96×10^{-4}	2.00×10^{-4}	2.08×10^{-4}
$\alpha_s = \langle C_{out}\rangle_D / \langle C_{out}\rangle_A$	45.663	43.950	41.779
$\alpha_p = \langle C_{out}\rangle_A / C_{in,A}$	0.196	0.200	0.208
L_{cond} [mol]	0.0500	0.0499	0.0510
$L_{cond}/(C_{in}\tau_A G_A)$ [%]	20.32	20.45	20.98
Q_{el} [KJ]	19.626	16.735	15.433
Q_{el}/L_{cond} [KJ/mol]	392.52	335.37	302.61
τ_D [s]	224	158	122
τ_A [s]	2460	2440	2430

constants, although, strictly speaking they change with the velocity and/or composition and/or temperature, and consequently, with time and space coordinates. These relations can be included in the model, although that would increase its complexity and introduce additional coupling of the equations. Second, the heat capacity and resistance of the adsorber wall were neglected, although, they generally should be taken into account. In order to do that, another sub-domain has to be added, with one application mode (Heat transfer by conduction) defined in it. Also, the heat transfer by radiation was not taken into account, although for the temperatures of the adsorbent bed during desorption, it should probably not be neglected.

In the next generation of multiphysics models of the ESA system we are planning to gradually upgrade the complexity by taking into account all these aspects.

Multiphysics modeling of more complex adsorbers with two and four cartridges is also in progress.

Acknowledgements Effort sponsored by the Air Force Office of Scientific Research, Air Force Material Command, USAF, under grant number FA8655-04-1-3053. This work was also partly supported by the Serbian Ministry of Science in the frame of Project No. 142014G.

Appendix 1: The model equations

8.1 Momentum balances and continuity equations for the gas phase

For the central tube and the annular space between the cartridge and the adsorber wall (sub-domains S-1 and S-3):

$$r\rho_g\frac{\partial u}{\partial t}+\nabla\left[-2r\mu\frac{\partial u}{\partial r}-r\mu\left(\frac{\partial u}{\partial z}+\frac{\partial v}{\partial r}\right)\right]=-\left(r\left(\rho_g\left(u\frac{\partial u}{\partial r}+v\frac{\partial u}{\partial z}\right)+\frac{\partial p}{\partial r}\right)+2\mu\frac{u}{r}\right), \tag{7}$$

$$r\rho_g\frac{\partial v}{\partial t}+\nabla\left[-r\mu\left(\frac{\partial v}{\partial r}+\frac{\partial u}{\partial z}\right)-2r\mu\frac{\partial v}{\partial z}\right]=-r\left(\rho_g\left(u\frac{\partial v}{\partial r}+v\frac{\partial v}{\partial z}\right)+\frac{\partial p}{\partial z}\right), \tag{8}$$

$$-\left(\rho_g\left(r\left(\frac{\partial u}{\partial r}+\frac{\partial v}{\partial z}\right)+u\right)+\frac{\partial\rho_g}{\partial r}u+\frac{\partial\rho_g}{\partial z}v\right)=0. \tag{9}$$

For the adsorbent bed (sub-domain S-2):

$$r\rho_g\frac{\partial u}{\partial t}+\nabla\left[-2r\mu\frac{\partial u}{\partial r}+\left(-r\mu\left(\frac{\partial u}{\partial z}+\frac{\partial v}{\partial r}\right)\right)\right]=-\left(r\left(\frac{\mu}{k}u+\frac{\partial p}{\partial r}\right)+2\mu\frac{u}{r}\right), \tag{10}$$

$$r\rho_g\frac{\partial v}{\partial t}+\nabla\left[-r\mu\left(\frac{\partial v}{\partial r}+\frac{\partial u}{\partial z}\right)-2r\mu\frac{\partial v}{\partial z}\right]=-r\left(\frac{\mu}{k}v+\frac{\partial p}{\partial z}\right), \tag{11}$$

$$-\left(\rho_g\left(r\left(\frac{\partial u}{\partial r}+\frac{\partial v}{\partial z}\right)+u\right)+\frac{\partial\rho_g}{\partial r}u+\frac{\partial\rho_g}{\partial z}v\right)=0. \tag{12}$$

The gas density is calculated as:

$$\rho_g=\frac{p}{R_gT_g(1+C)}, \tag{13}$$

8.2 Heat balances for the gas phase

For the central tube and the annular space between the cartridge and the adsorber wall (S-1 and S-3):

$$r\frac{\partial}{\partial t}\left[\rho_g(c_{pg}+c_{pv}C)T_g\right]+\nabla\left(-rD_{t,r}^{hg}\frac{\partial T_g}{\partial r}-rD_{t,z}^{hg}\frac{\partial T_g}{\partial z}\right)=-r\rho_gc_{pv}T_g\left(u\frac{\partial C}{\partial r}+v\frac{\partial C}{\partial z}\right)-r\rho_g(c_{pg}+c_{pv}C)u\frac{\partial T_g}{\partial r}-r\rho_g(c_{pg}+c_{pv}C)v\frac{\partial T_g}{\partial z}. \tag{14}$$

For the adsorbent bed (S-2):

$$r\frac{\partial}{\partial t}\left[\rho_g(c_{pg}+c_{pv}C)T_g\right]+\nabla\left(-rD_{t,r,b}^{hg}\frac{\partial T_g}{\partial r}-rD_{t,z,b}^{hg}\frac{\partial T_g}{\partial z}\right)=r\left(h_ba(T_s-T_g)-\rho_gc_{pv}T_g\left(u\frac{\partial C}{\partial r}+v\frac{\partial C}{\partial z}\right)\right)-r\rho_g(c_{pg}+c_{pv}C)u\frac{\partial T_g}{\partial r}-r\rho_g(c_{pg}+c_{pv}C)v\frac{\partial T_g}{\partial z}. \tag{15}$$

8.3 Adsorbate balances for the gas phase

For the central tube and the annular space between the cartridge and the adsorber wall (S-1 and S-3):

$$r\frac{\partial C}{\partial t}+\nabla\left(-r\frac{D_{m,r}}{\rho_g}\frac{\partial C}{\partial r}-r\frac{D_{m,z}}{\rho_g}\frac{\partial C}{\partial z}\right)=-\left(ru\frac{\partial C}{\partial r}+rv\frac{\partial C}{\partial z}\right). \tag{16}$$

For the adsorbent bed (S-2):

$$r\frac{\partial C}{\partial t}+\nabla\left(-r\frac{D_{m,r,b}}{\rho_g}\frac{\partial C}{\partial r}-r\frac{D_{m,z,b}}{\rho_g}\frac{\partial C}{\partial z}\right)=r\frac{k_ma}{\rho_g}(C^*-C)-\left(ru\frac{\partial C}{\partial r}+rv\frac{\partial C}{\partial z}\right). \tag{17}$$

8.4 Electric current balance for resistive heating (S-2)

$$\nabla\left(-r\frac{1}{\rho}\frac{\partial U}{\partial r}-r\frac{1}{\rho}\frac{\partial U}{\partial z}\right)=0. \tag{18}$$

Linear temperature dependence of the electric resistivity of the adsorbent material, which was obtained experimentally for ACFC adsorbent (Sullivan 2003) is used:

$$\rho=\rho_0(1+b(T_s-T_R)). \tag{19}$$

8.5 Heat balance for the solid phase within the adsorbent bed (S-2)

$$r\rho_b\frac{\partial}{\partial t}\left[(c_{ps}+c_{pl}q)T_s\right]-\nabla\left(rD_{t,r}^{hs}\frac{\partial T_s}{\partial r}+rD_{t,z}^{hs}\frac{\partial T_s}{\partial z}\right)$$
$$=r\frac{\delta\dot{Q}_{el}}{dV}+r\rho_b\Delta H_{ads}\frac{\partial q}{\partial t}-rh_ba(T_s-T_g), \tag{20}$$

$$\frac{\delta\dot{Q}_{el}}{dV}=\frac{1}{\rho}\left(\left(\frac{\partial U}{\partial r}\right)^2+\left(\frac{\partial U}{\partial z}\right)^2\right)$$
$$=\frac{1}{\rho_0(1+b(T_s-T_R))}\left(\left(\frac{\partial U}{\partial r}\right)^2+\left(\frac{\partial U}{\partial z}\right)^2\right). \tag{21}$$

8.6 Adsorbate balance for the solid phase within the adsorbent bed (S-2)

$$\rho_b\frac{\partial q}{\partial t}=k_ma(C-C^*). \tag{22}$$

8.7 Equilibrium relation

Based on Dubinin–Radushkevich equation (Dubinin 1989), a relation between the equilibrium adsorbate concentration in the gas phase C^* and its concentration in the solid phase q and temperature T_s is obtained:

$$C^*=\frac{p^o}{p}\exp\left[-\frac{E}{R_gT_s}\sqrt{-\ln\left(\frac{M_Aq}{\rho_AW_0}\right)}\right]. \tag{23}$$

Wagner equation (Reid et al. 1987) is used to calculate the adsorbate saturation pressure p^o, needed in (23):

$$\ln\left(\frac{p^o}{p_c}\right)=\left(\frac{VP_Ax+VP_Bx^{1.5}+VP_Cx^3+VP_Dx^6}{1-x}\right),$$
$$x=1-(T_s/T_c). \tag{24}$$

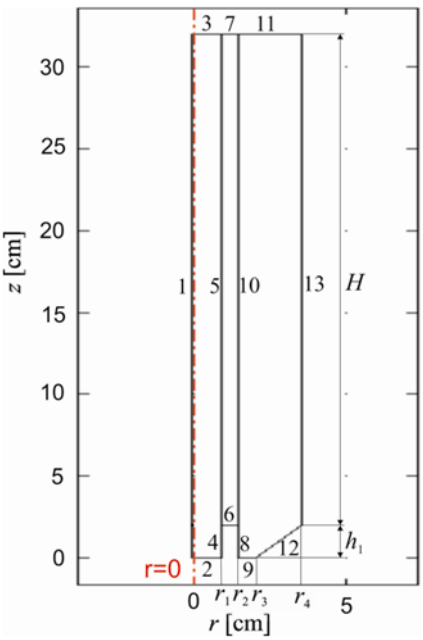

Fig. 10 Definition of the boundaries

8.8 Boundary conditions

For better clarity, in Fig. 10 we show the cartridge geometry in which all boundaries between the sub-domains, or between the adsorber and the surrounding are defined and numbered (from 1 to 13). The boundary conditions defined at these boundaries are:

Boundary 1—This is the axis of symmetry: no momentum, mass or heat transfer through it.

Boundary 2:

$$z=0,\qquad r\in(0,r_1):\qquad u=0,\qquad v=\frac{G}{r_1^2\pi\rho_g},$$
$$T_g=T_{gin},\qquad C=C_{in}. \tag{25}$$

Boundary 3:

$$z=H+h_1,\qquad r\in(0,r_1):\qquad u=0,\qquad v=0,$$
$$-D_{t,z}^{hg}\frac{\partial T_g}{\partial z}=0,\qquad -D_{m,z}\frac{\partial C}{\partial z}=0. \tag{26}$$

Boundary 4:

$$z\in(0,h_1),\qquad r=r_1:\qquad u=0,\qquad v=0,$$
$$-D_{tr}^{hg}|_{it}\frac{\partial T_g}{\partial z}=0,\qquad -D_{mr}|_{it}\frac{\partial C}{\partial z}=0. \tag{27}$$

Boundary 5:

$$
\begin{aligned}
&r = r_1, \qquad z \in (h_1, h_1 + H): \qquad p|_{ct} = p|_b,\\
&u|_{ct} = u|_b, \qquad v|_{ct} = v|_b,\\
&\left(-D_{t,r}^{hg}\frac{\partial T_g}{\partial r} + \rho_g(c_{pg} + c_{pv}C)uT_g\right)_{ct}\\
&\quad = \left(-D_{t,r,b}^{hg}\frac{\partial T_g}{\partial r} + \rho_g(c_{pg} + c_{pv}C)uT_g\right)_b\\
&\qquad + h_{s1}(1-\varepsilon_b)(T_s - T_g),\\
&\left(-D_{m,r}\frac{\partial C}{\partial r} + uC\right)_{ct}\\
&\quad = \left(-D_{m,r,b}\frac{\partial C}{\partial r} + uC\right)_b + k_{m1}(1-\varepsilon_b)(C^* - C),\\
&-D_{t,r}^{hs}\frac{\partial T_s}{\partial r} = h_{s1}(T_g - T_s), \qquad J = 0.
\end{aligned}
\tag{28}
$$

Boundary 6:

$$
\begin{aligned}
&z = h_1, \qquad r \in (r_1, r_2): \qquad u = 0, \qquad v = 0,\\
&-D_{t,z,b}^{hg}\frac{\partial T_g}{\partial z} = 0, \qquad -D_{m,z,b}\frac{\partial C}{\partial z} = 0,\\
&U = U_0, \qquad -D_{tz}^{hs}\frac{\partial T_s}{\partial z} = 0.
\end{aligned}
\tag{29}
$$

Boundary 7:

$$
\begin{aligned}
&z = h_1 + H, \qquad r \in (r_1, r_2): \qquad u = 0, \qquad v = 0,\\
&-D_{t,z,b}^{hg}\frac{\partial T_g}{\partial z} = 0, \qquad -D_{m,z,b}\frac{\partial C}{\partial z} = 0,\\
&U = 0, \qquad D_{tz}^{hs}\frac{\partial T_s}{\partial z} = 0.
\end{aligned}
\tag{30}
$$

Boundary 8:

$$
\begin{aligned}
&z \in (0, h_1), \qquad r = r_2: \qquad u = 0, \qquad v = 0,\\
&-D_{t,r}^{hg}\frac{\partial T_g}{\partial z} = 0, \qquad -D_{m,r}\frac{\partial C}{\partial z} = 0.
\end{aligned}
\tag{31}
$$

Boundary 9:

$$
\begin{aligned}
&z = 0, \qquad r \in (r_2, r_3): \qquad p|_{as} = p_a,\\
&-D_{t,z}^{hg}\frac{\partial T_g}{\partial z} = 0, \qquad -D_{m,z}\frac{\partial C}{\partial z} = 0.
\end{aligned}
\tag{32}
$$

Boundary 10:

$$
\begin{aligned}
&r = r_2, \qquad z \in (h, h + H): \qquad p|_b = p|_{as},\\
&u|_b = u|_{ot}, \qquad v|_b = v|_{as},\\
&\left(-D_{t,r,b}^{hg}\frac{\partial T_g}{\partial r} + \rho_g(c_{pg} + c_{pv}C)uT_g\right)_b\\
&\quad = \left(-D_{t,r}^{hg}\frac{\partial T_g}{\partial r} + \rho_g(c_{pg} + c_{pv}C)uT_g\right)_{ot}\\
&\qquad + h_{s2}(1-\varepsilon_b)(T_s - T_g),\\
&\left(-D_{m,r,b}\frac{\partial C}{\partial r} + uC\right)_b\\
&\quad = \left(-D_{m,r}\frac{\partial C}{\partial r} + uC\right)_{ot} + k_{m2}(1-\varepsilon_b)(C^* - C),\\
&J = 0, \qquad -D_{t,r}^{hs}\frac{\partial T_s}{\partial r} = h_{s2}(T_g - T_s).
\end{aligned}
\tag{33}
$$

Boundary 11:

$$
\begin{aligned}
&z = h + H, \qquad r \in (r_2, r_4): \qquad u = 0, \qquad v = 0,\\
&-D_{t,z}^{hg}\frac{\partial T_g}{\partial z} = 0, \qquad -D_{m,z}\frac{\partial C}{\partial z} = 0.
\end{aligned}
\tag{34}
$$

Boundaries 12 and 13—These boundaries correspond to the outer wall of the adsorber. The boundary conditions corresponding to this surface are different for the cases without and with condensation.

- For Model_A and Model_D (adsorption and desorption without condensation):

$$
\begin{aligned}
&r = r_4, \qquad z \in (h, h + H) \quad \text{and} \quad r \in (r_3, r_4),\\
&z \in (0, h): \qquad u = 0, \qquad v = 0,\\
&-D_{m,r}\frac{\partial C}{\partial z} = 0, \qquad -D_{t,r}^{hg}\frac{\partial T_g}{\partial r} = h_{wg}(T_g - T_a).
\end{aligned}
\tag{35}
$$

- For Model_DC (desorption with condensation):

$$
\begin{aligned}
&r = r_4, \qquad z \in (h, h + H) \quad \text{and}\\
&r \in (r_3, r_4), z \in (0, h):\\
&u = 0, \qquad v = 0, \qquad C = C_{sat}(T_w),\\
&-D_{t,r}^{hg}\frac{\partial T_g}{\partial r} = -D_{m,r}\frac{\partial C}{\partial r}(-\Delta H_{cond}) + h_{wg}(T_g - T_a).
\end{aligned}
\tag{36}
$$

Appendix 2: Definitions and values of the model parameters used for simulation

All transport coefficients and physical parameters used in the models were considered as constants. The values of the

Table 4

Parameter	Notation and value
Adsorber dimensions (defined in Fig. 2)	$r_1 = 0.95$ cm, $r_2 = 1.5$ cm
	$r_3 = 2$ cm, $r_4 = 3.5$ cm
	$H = 30$ cm, $h_1 = 2$ cm
Bed porosity [5]	$\varepsilon_b = 0.72$
Specific surface area for heat and mass transfer [5]	$a = 13.65\ \text{cm}^2/\text{cm}^3$
Ambient pressure	$p_{\text{atm}} = 101325$ Pa
Inlet gas temperature	$T_{gin} = 293.15$ K
Ambient temperature	$T_a = 293.15$ K
Wall temperature	$T_w = 293.15$ K
Bed hydraulic permeability [5]	$k = 4.59 \times 10^{-6}\ \text{cm}^2$
Mass transfer coefficient within the bed [1]	$k_m = 0.0003\ \text{mol}/(\text{cm}^2\ \text{s})$
Bed to central tube mass transfer coefficient [1]	$k_{m1} = 0.0003\ \text{mol}/(\text{cm}^2\ \text{s})$
Bed to annular tube mass transfer coefficient [1]	$k_{m2} = 0.0003\ \text{mol}/(\text{cm}^2\ \text{s})$
Heat transfer coefficient within the bed [1, 2]	$h_b = 0.0055\ \text{W}/(\text{cm}^2\ \text{s})$
Bed to central tube heat transfer coefficient [3]	$h_{s1} = 0.001\ \text{W}/(\text{cm}^2\ \text{s})$
Bed to central tube heat transfer coefficient [3]	$h_{s2} = 0.001\ \text{W}/(\text{cm}^2\ \text{s})$
Heat transfer coefficient defining heat losses [3]	$h_{wg} = 5 \times 10^{-5}\ \text{W}/(\text{cm}^2\ \text{K})$
Axial and radial dispersion coefficient of the gas phase in the central tube and annular space [2]	$D_{m,z} = D_{m,r} = 1\ \text{mol}/(\text{cm}\ \text{s})$
Axial and radial dispersion coefficient of the gas phase in the adsorbent bed [2]	$D_{m,z,b} = D_{m,z,b} = 8 \times 10^{-5}\ \text{mol}/(\text{cm}\ \text{s})$
Axial and radial heat diffusivity of the gas phase in the central tube and annular space [4]	$D_{t,z}^{hg} = D_{t,r}^{hg} = 1\ \text{W}/(\text{K}\ \text{cm})$
Axial and radial heat diffusivity of the gas phase in the adsorbent bed [4]	$D_{t,z,b}^{hg} = D_{t,r,b}^{hg} = 0.00014\ \text{W}/(\text{K}\ \text{cm})$
Axial and radial heat diffusivity of the solid phase [4]	$D_{t,r}^{hs} = D_{t,r}^{hs} = 0.0012\ \text{W}/(\text{cm}\ \text{K})$
Molar heat of adsorption [5]	$(-\Delta H_{ads}) = 66200\ \text{J/mol}$
Molar heat of condensation [5]	$(-\Delta H_{cond}) = 31230\ \text{J/mol}$
Adsorbent bed density [5]	$\rho_b = 0.221\ \text{g/cm}^3$
Adsorbate density [5]	$\rho_A = 0.81\ \text{g/cm}^3$
Adsorbate molar mass	$M_A = 72.107\ \text{g/mol}$
Inert gas molar mass (nitrogen)	$M_B = 28.02\ \text{g/mol}$
Specific heat capacity of liquid adsorbate [5]	$c_{pl} = 157.9\ \text{J}/(\text{mol}\ \text{K})$
Specific heat capacity of the inert gas [5]	$c_{pg} = 29.13\ \text{J}/(\text{mol}\ \text{K})$
Heat capacity of the solid phase [5]	$c_{ps} = 0.71\ \text{J}/(\text{g}\ \text{K})$
Specific heat capacity of gaseous adsorbate [5]	$c_{pv} = 100.9\ \text{J}/(\text{mol}\ \text{K})$
Dynamic viscosity of the inert gas [1]	$\mu = 1.78 \times 10^{-4}\ \text{g/cm/s}$
Electric resistivity at referent temperature $T_R = 293$ K [5]	$\rho_0 = 0.202\ \Omega\,\text{cm}$
Temperature coefficient of the bed electrical resistivity [5]	$b = -2 \times 10^{-3}\ 1/\text{K}$
Critical temperature of the inert gas (nitrogen) [5]	$T_{cB} = 126.2$ K
Critical pressure of the adsorbate [5]	$p_{cA} = 4.26 \times 10^6$ Pa
Critical pressure of the inert gas (nitrogen) [5]	$p_{cB} = 3.39 \times 10^6$ Pa
Wagner constants for the adsorbate [5]	$VP_A = -7.71476$, $VP_B = 1.71061$
	$VP_C = -3.6877$, $VP_D = -0.75169$
Total volume of micropores (D-R equation) [5]	$W_0 = 0.748\ \text{cm}^3/\text{g}$
Adsorption energy of the adsorbate (D-R equation) [5]	$E = 14.43 \times 10^3\ \text{J/mol}$

Literature sources: [1] Perry and Green (1997), [2] Ruthven (1984), [3] Incropera and DeWitt (1996), [4] Fuentes et al. (1998), [5] Sullivan (2003)

transport coefficients were estimated using literature correlations (defined by the number in brackets) for some average conditions during the process. The values of the physical parameters are also taken from literature (given in brackets) and correspond to some average conditions.

References

Azou, A., Martin, G., Le Cloirec, P.: Improvement of a closed cycle for removal and recovery of dilute gases—application to dry cleaning industry. Environ. Technol. **14**, 471–478 (1993)

Baudu, M., Le Cloirec, P., Martin, G.: La regeneration par echauffement intrinseque de charbons actifs utilises pour le traitement d'air. Environ. Technol. **13**, 423–435 (1992)

Bathen, D.: Gasphasen—Adsorption in der Umwelttechnik—Stand der Technik und Perspektiven. Chemie Ingenieur Technik **74**, 209–216 (2002)

Bathen, D., Schmidt-Traub, H., Stube, J.: Experimenteller Vorgleich verschiedener thermischer Desorptionsverfahren zur Losungsmittel ruckgewinnung. Chemie Ingenieur Technik **69**, 132–134 (1997)

Comsol AB: Comsol Documentation, Comsol Multiphysics Users Guide (2005)

Dubinin, M.M.: Fundamentals of the theory of adsorption in micropores of carbon adsorbents: characteristics of their adsorption properties and microporous structures. Carbon **27**, 457–467 (1989)

Fabuss, B.M., Dubois, W.H.: Carbon adsorption-electrodesorption process. In: 63rd Annual Meeting of the Air Pollution Control Association, St. Louis, MO (1970)

Fuentes, J., Pironti, F., Lopez de Ramos, A.L.: Effective thermal conductivity in a radial-flow packed-bed reactor. Int. J. Thermophys. **19**, 781–792 (1998)

Incropera, F.P., DeWitt, D.P.: Fundamentals of Heat and Mass Transfer. Wiley, New York (1996)

Lordgooei, M., Carmichael, K.R., Kelly, T.W., Rood, M.J., Larson, S.M.: Activated carbon cloth adsorption—cryogenic system to recover toxic volatile organic compound. Gas Sep. Purif. **10**, 123–130 (1996)

Luo, L., Ramirez, D., Rood, M., Grevillot, G., Hay, J., Thurston, D.: Adsorption and electrothermal desorption of organic vapors using activated carbon adsorbents with novel morphologies. Carbon **44**, 2715–2723 (2006)

Moon, S.H., Shim, J.W.: A novel process for CO2/CH4 gas separation on activated carbon fibers—electric swing adsorption. J. Colloid Interface Sci. **298**, 523–528 (2006)

Petkovska, M., et al.: Temperature-swing gas separation with electrothermal desorption step. Sep. Sci. Technol. **26**, 425–444 (1991)

Petkovska, M., Antov, D., Sullivan, P.: Electrothermal desorption in an annular-radial flow-ACFC adsorber-mathematical modeling. Adsorption **11**(1 Suppl.), 585–590 (2005)

Petkovska, M., Mitrović, M.: Microscopic modeling of electrothermal desorption. Chem. Eng. J. Biochem. Eng. J. **53**, 157–165 (1994a)

Petkovska, M., Mitrović, M.: One-dimensional, non-adiabatic, microscopic model of electrothermal desorption process dynamics. Chem. Eng. Res. Des. **72**, 713–722 (1994b)

Perry, R.H., Green, D.W.: Perry's Chemical Engineer's Handbook, 7th edn. McGraw–Hill, New York (1997)

Reid, R.C., Prausnitz, J.M., Poling, B.: The Properties of Gases & Liquids. McGraw–Hill, New York (1987)

Rood, M., et al.: Selective sorption and desorption of gases with electrically heated activated carbon fiber cloth element. US Patent No. 6,346,936 B1 (2002)

Ruthven, D.M.: Principles of Adsorption and Adsorption Processes. Wiley, New York (1984)

Snyder, J.D., Leesch, J.G.: Methyl bromide recovery on activated carbon with repeated adsorption and electrothermal regeneration. Ind. Eng. Chem. Res. **40**, 2925–2933 (2001)

Subrenat, A., Le Cloirec, P.: Industrial application of adsorption onto activated carbon cloths and electro-thermal regeneration. J. Environ. Eng. **130**, 249–257 (2004)

Subrenat, A.S., Le Cloirec, P.A.: Volatile organic compound (VOC) removal by adsorption onto activated carbon fiber cloth and electrothermal desorption: An industrial application. Chem. Eng. Commun. **193**, 478–486 (2006)

Sullivan, P.: Organic vapor recovery using activated carbon fiber cloth and electrothermal desorption. Ph.D. thesis, University of Illinois at Urbana-Champaign (2003)

Sullivan, P.D., Rood, M.J., Hay, K.J., Qi, S.: Adsorption and electrothermal desorption of hazardous organic vapors. J. Environ. Eng. **127**, 217–223 (2001)

Sullivan, P.D., Rood, M.J., Grevillot, G., Wander, J.D., Hay, K.J.: Activated carbon fiber cloth electrothermal swing adsorption system. Environ. Sci. Technol. **38**, 4865–4877 (2004a)

Sullivan, P.D., Rood, M.J., Dombrowski, K.D., Hay, K.J.: Capture of organic vapors using adsorption and electrothermal regeneration. J. Environ. Eng. **130**, 258–267 (2004b)

Sushchev, S.V., Shumyatskii, Y.I., Alekhina, M.B.: Steady-state temperature and adsorption distributions in a resistance-heated granular activated-charcoal bed. Theor. Found. Chem. Eng. **36**, 141–144 (2002)

Yu, F.D., Luo, L.A., Grevillot, G.: Adsorption isotherms of VOCs onto an activated carbon monolith: experimental measurement and correlation with different models. J. Chem. Eng. Data **47**, 467–473 (2002)

Yu, F.D., Luo, L., Grevillot, G.: Electrothermal swing adsorption of toluene on an activated carbon monolith: experiments and parametric theoretical study. Chem. Eng. Proc. **46**, 70–81 (2007)